ELSEVIER

Journal of Molecular Catalysis A: Chemical 193 (2003) 121–137

JOURNAL OF MOLECULAR CATALYSIS A: CHEMICAL

www.elsevier.com/locate/molcata

A combined theoretical and experimental study of NO decomposition on Pd and Pd-Mo catalysts

G.M. Tonetto, M.L. Ferreira*, D.E. Damiani

PLAPIQUI (UNS-CONICET), Camino La Carrindanga km 7, CC 717, 8000 Bahia Blanca, Argentina

Received 6 March 2002; accepted 17 July 2002

Abstract

Studies of NO decomposition on Pd/γ-Al_2O_3, Mo/γ-Al_2O_3 and Pd-Mo/γ-Al_2O_3 catalysts were made. The reaction was investigated at 400 °C using a reactant mixture of 1100 ppm NO in He. Adsorption and dissociation of NO, O_2 and N_2 on Pd(1 1 1), MoO_x-Pd(1 1 1) and MoO_x-γAl_2O_3 surfaces have been investigated using a molecular orbital approach of the extended Hückel (EHMO) type, including repulsion terms.

The catalytic tests have revealed that the binary catalyst present a different behavior for the NO decomposition, the main difference being a longer steady-state activity at low temperature. Characterization results by TPR and hydrogen chemisorption have indicated that palladium physicochemical properties are altered by an effective interaction with molybdenum. This interaction appears to be responsible for the observed modification in NO activity.

Our results of EHMO have showed that the NO adsorption energy on MoO_x-Pd(1 1 1) model is lower than the one for Pd(1 1 1) or MoO_x-γAl_2O_3. Also, adsorption and dissociation of N_2 and O_2 are notoriously modified when an interaction between the two metals exists. Those results would indicate the existence of a Pd–Mo interface with catalytic properties different to the metals.

Keywords: NO decomposition; Pd catalyst; Pd-Mo catalyst

1. Introduction

Nitrogen oxides (NO_x), the term used to describe the sum of NO, NO_2 and other oxides of nitrogen, play a main role in air pollution. The major sources of man-made NO_x emissions are high-temperature combustion processes, such as those occurring in automobiles and power plants.

NO_x have serious effects on human health and they can cause serious injure to vegetation and animals. At ground level, ozone is formed when NO_x and volatile organic compounds (VOCs) react in the presence of sunlight. Also, oxides of nitrogen are precursors to acidic precipitation, which may affect both terrestrial and aquatic ecosystems.

For these reasons, it is indispensable, the elimination of the nitrogen oxides of gaseous shams. Choosing the catalyst for NO elimination depends on different purposes and reaction media. It is possible to classify the processes in five categories:

- NO selective catalytic reduction with ammonia (NH_3-SCR) typical in chemical industries and plants of energy generation.
- NO catalytic reduction in the presence of CO and/or hydrogen, typical in control of automobile pollution.

* Corresponding author.
E-mail address: caferrei@criba.edu.ar (M.L. Ferreira).

1381-1169/02/$ – see front matter © 2002 Published by Elsevier Science B.V.
PII: S1381-1169(02)00444-2

- NO selective catalytic reduction (SCR) in the presence of hydrocarbons, that has still not reached industrial use but it can be applied for control of the automobile contamination and in several industrial plants.
- Direct decomposition of NO, which is an important goal since it eliminates the need of reducing agents.
- Catalytic traps of NO_x, promote the oxidation of NO to NO_2 over a noble metal followed by reaction between NO_2 and an oxide (BaO typically) to form nitrate. It has special application in diesel motors.

Direct decomposition of nitric oxide by catalysts has been considered to be the best NO removal technique from exhaust stream because nitrogen monoxide is thermodynamically unstable relative to N_2 and O_2 at low temperatures (between 20 and 700 °C). However, no suitable catalyst with sustainable high activity has been found, since oxygen obtained by NO decomposition is strongly bonded to the catalyst surface, poisoning active sites and preventing further NO dissociation [1,2].

Cu-ZSM-5 catalysts have showed the highest activity for the direct NO decomposition among various analyzed catalysts [3,4]. However, the narrow temperature window of operation for Cu-ZSM-5, its rapid deactivation by water and susceptibility to SO_2 poisoning severely limit its practical use.

Also, it must be consider that the study of NO decomposition reaction is important because the reaction for NO removal on catalysts containing noble metals is described in terms of NO adsorption and dissociation, followed by oxygen elimination from catalyst surface by reaction with a reducing agent [5–8]. There are many publications about supported Pd catalysts associated with the removal of NO in automotive exhausts [9–13]. Gandhi et al. [14] were among the first in the use of molybdenum, due to its promoting effect in automotive three-way catalysts. Halaz et al. [15–17] studied the catalytic reduction of nitric oxide by CO, H_2 and CO–H_2 on Pd-Mo/γ-Al_2O_3. They have reported that at higher temperatures molybdenum could improve the performance of the catalyst, especially at slightly oxidizing conditions. Schmal et al. [18] have confirmed the high selectivity for N_2 in the CO and NO reaction on Pd-Mo/γ-Al_2O_3. Based on TPD analysis of NO and CO adsorption, a redox mechanism for NO reduction to N_2 involving partially reduced molybdenum oxide was proposed. The same group [19] has studied the effect of MoO_3 on Pd/γ-Al_2O_3 catalysts for the reduction of NO by methane and demonstrated that the selectivity towards N_2 was enhanced due to the promoting effect of NO decomposition on the MoO_x surface.

The objective of this work is to examine the effects of Mo on the activity of Pd catalysts for NO decomposition. Experimental results about NO decomposition reaction over Pd/γ-Al_2O_3, Mo/γ-Al_2O_3 and Pd-Mo/γ-Al_2O_3 catalysts are presented and discussed. This paper also reports the result of the study of adsorption and dissociation of NO, O_2 and N_2 on Pd(1 1 1), MoO_x-Pd(1 1 1) and MoO_x-γAl_2O_3 model surfaces using a molecular orbital approach of the extended Hückel (EHMO) type, including repulsion terms.

2. Experimental

2.1. Catalysts preparation

The support material was γ-Al_2O_3 (Condea, Puralox; 148 $m^2\,g^{-1}$). Prior to impregnation, alumina was dried under N_2 at 150 °C for 2 h.

Pd/γ-Al_2O_3 catalyst was prepared by wet impregnation of Al_2O_3 with a solution of $Pd(C_5H_7O_2)_2$ (Alfa) in toluene (Merck). Mo/γ-Al_2O_3 catalyst was obtained by incipient-wetness impregnation of alumina with a solution of $Mo_7O_{24}(NH_4)_6{\cdot}4H_2O$ (Alfa), at pH 7. After impregnation, both the samples were dried in Ar at 150 °C for 2 h and then calcined in air (chromatographic grade) at 500 °C during 2 h.

Table 1
Characterization of catalysts

Catalyst	Metal loading (wt.%)		Preparation	Pd_{exp} [a]
	Pd	Mo		
Pd/γ-Al_2O_3	0.82	–	w.i.[b]	0.55
Mo/γ-Al_2O_3	–	0.50	i.w.i.[c]	–
Pd-Mo/γ-Al_2O_3	0.74	0.50	i.w.i.–w.i. sequence	0.51
Mo-Pd/γ-Al_2O_3	0.82	0.88	w.i.–i.w.i. sequence	0.46

[a] Fraction of exposed palladium.
[b] w.i., wet impregnation.
[c] i.w.i., incipient-wetness impregnation.

The bimetallic samples were prepared by impregnation in sequence utilizing the same precursors. Pd-Mo/γ-Al_2O_3 catalyst was obtained by wet impregnation of Mo/γ-Al_2O_3 with a solution of $Pd(C_5H_7O_2)_2$. Mo-Pd/γ-Al_2O_3 refers to catalysts prepared by incipient-wetness impregnation of Pd/γ-Al_2O_3 with a solution of $Mo_7O_{24}(NH_4)_6{\cdot}4H_2O$. After impregnation the samples were dried and calcinated similar to monometallic catalysts.

The prepared catalysts and their metal loading, as measured by atomic absorption spectroscopy, are given in Table 1.

2.2. H_2 chemisorption

The chemisorption uptakes were measured in a conventional glass apparatus [20]. Before reduction, the catalysts were oxidized in air at 500 °C for 1 h. Then, the samples were purged in He and reduced at 250 °C in flowing H_2 for 1 h. Following reduction, the samples were evacuated for 20 h at reduction temperature and cooled to adsorption temperature (25 °C) under vacuum. Irreversible uptakes were determined from dual hydrogen adsorption isotherms measured using the method of Benson et al. [21]. The fraction of exposed palladium was calculated assuming that one hydrogen atom is adsorbed per surface of palladium atom.

2.3. TPR experiments

TPR experiments were performed in a conventional apparatus, as described previously [22]. Before reduction, the catalysts were oxidized in flowing chromatographic air at 300 °C for 1 h and purged and cooled in Ar. Then a mixture of 5% hydrogen in argon flow was passed through the sample and the temperature was raised from −50 to 500 °C at a heating rate of 10 °C min^{-1}.

2.4. Catalytic activity measurements

The catalysts were tested in a horizontal glass-made packed bed reactor (6 mm o.d.) placed in an electrically heated oven. The reaction products were analyzed by on-line gas chromatography operating in the TCD mode. Two Porapak Q columns operated isothermally at 40 and −20 °C with He as carrier gas were used for separation.

Prior to each activity measurement, the catalysts were pretreated in situ in 5% H_2 in Ar mixture. The reaction mixture contains 1100 ppm of NO in balance He. Catalyst weight was adjusted in order to keep constant the weight of palladium in the different experiments. The reaction mixture flow rate was maintained at 35 cm^3 min^{-1} and the catalytic bed temperature at 400 °C.

3. Theoretical model

The theoretical studies applied to catalysis may be classified in semi-empirical and ab initio methods. Amongst the formers, an EHMO method was selected to perform the quantum mechanical study of the Pd and Pd-Mo catalytic systems.

The EHMO was widely used by Hoffman [23], Sumerville and Hoffman [24] and Hoffman et al. [25] to study electronic structure of transition metal complexes and adsorbed molecules, it provides useful qualitative trends in large system models. The electronic structure and derived properties are established from electron equations for the molecular orbitals, approximated by experimental data. In this formalism, the non-diagonal elements of Hamiltonian of the system are proportional to the overlap matrix elements. More recently, Chamber et al. [26] and Anderson and Hoffmann [27] introduced some corrections were in order to improve the traditional extended Hückel–Hamiltonian.

The total energy of a selected adsorbed molecule on a palladium cluster is a sumatory of an attractive and a repulsive term and may be represented by the following equation:

$$E_t = \sum_i n_i E_i + \frac{1}{2}\sum_i \sum_{i \neq j} E_{rep(i,j)} \quad (1)$$

where the attractive energy is related to the electrons in the valence level i with an occupancy n_i. The repulsion energy is originated between all the possible pairs of nucleus i-fixed atom j.

Experimental parameters are necessary for calculations, being the EHMO a semi-empirical method. We have used reported ionization potential obtained from spectroscopic data [28]. Since for the level 4p only

Table 2
Atomic parameters used for EHMO calculation

Atom	Orbital	Ionization potential (eV)	Orbital exponents
Pd	5s	−7.24	2.19
	5p	−3.68	2.15
	4d	−11.90	5.98, 2.61, 0.55, 0.67
O	2s	−31.60	2.163
	2p	−16.78	2.750
H	1s	−13.60	1.00
Al	3s	−12.30	1.670
	3p	−6.50	1.383
N	2s	−26.00	1.8599
	2p	−13.40	1.8174
Mo	5s	9.10	2.256
	5p	5.92	1.956
	4d	10.06	4.542, 1.901

theoretical data are available in literature, we have taken the data of Hartree–Fock–Slater [29]. Parameters used in this work are presented in Table 2.

The program used to calculate the energy of the different adsorbed species was the ICONC, originally developed by Chamber et al. [26], which take into account repulsive terms that are not originally in the EHMO. In the present work, calculations were carried out with a modified version of ICONC. This version has been tested in previous work dealing with the adsorption of metallocenes and Ziegler–Natta catalysts [30,31].

The total energy of adsorbed species was calculated as the difference between the electronic energy of the system when the adsorbed molecule is at a finite distance from the surface and when the molecule is far away from the cluster surface. The geometry optimization was done at 0.1 Å step and due to the approximate nature of extended Hückel like methods the convergence criterion to the energy was set to 0.01 eV.

The dissociation energies shown in tables are defined as the total energy of dissociated species minus the total energies of adsorbed species. It could be considered as dissociation energy of adsorbed reactives. The semi-empirical MO calculations have been performed in the framework of the cluster approximation, that is the adsorption site and its neighborhood were modeled by a portion of the otherwise infinite solid.

4. Modeling of surface palladium structures

4.1. Surface Pd(1 1 1)

Since we do not have experimental information about the catalyst surface, the Pd(1 1 1) was the plane considered keeping in mind that Garbowski et al. [32] reported that 1.95 wt.% Pd/γ-Al_2O_3 catalyst presented a larger exhibition of Pd(1 1 1) plane after reduction in hydrogen at 500 °C.

A 74 atoms cluster was used to represent the Pd(1 1 1) face: 50 Pd and 24 H atoms. The atoms of hydrogen were used to complete the internal coordination of the palladium and to avoid the effect called “dangling bonds”. The palladium atoms were distributed in three layers of 19, 12 and 19 atoms as shown in Scheme 1.

Pd present an fcc structure with the cell parameter equal to 3.891 Å. This value leads to a triangular array

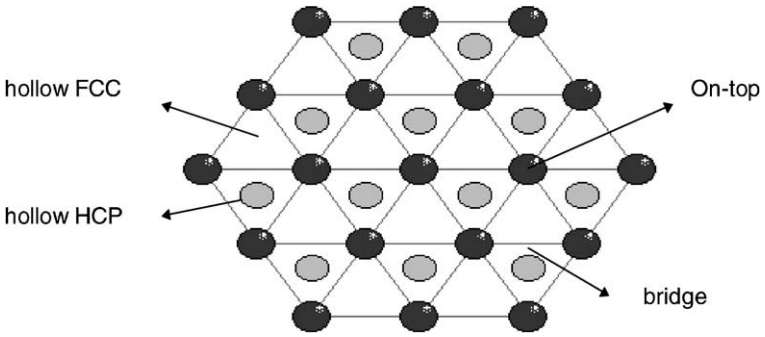

Scheme 1. Pd(1 1 1) model. First and second rows are depicted (open and filled circles, respectively).

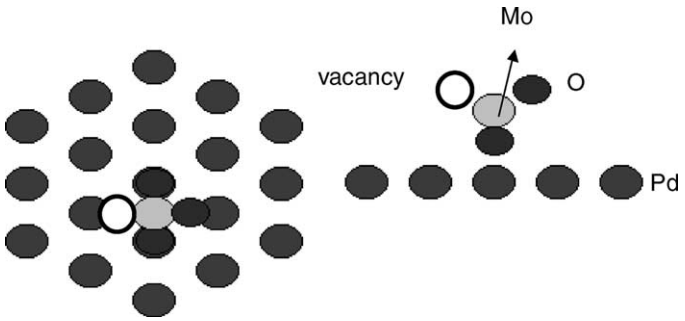

Scheme 2. MoO_x-Pd(1 1 1) model: top and lateral views. First Pd row is depicted.

(hexagonal close-packed) with a Pd–Pd distance of 2.70 Å. The separation between layers is 2.20 Å for the face (1 1 1) [33].

Keeping in mind previous results [34] we have worked without considering surface relaxation in all the calculations. This model will be identified as Pd(1 1 1).

4.2. Surface MoO_x-Pd(1 1 1)

A MoO_x species was introduced on the first layer of the Pd(1 1 1) cluster in order to represent the Pd-Mo catalytic system. A cluster of 78 atoms was modeled: 50 Pd, 1 Mo, 3 O and 24 H located as shown in Scheme 2.

Tetrahedral coordinating structure was assigned to MoO_x species because it is widespread accepted that the structure of molybdenum oxides supported on alumina depends on the metallic content [35–39]. It is assumed that Mo forms monomeric tetrahedral species when the metallic loading is smaller than 3–4%, while polymeric octahedral species appear at higher metallic loading. Crystalline MoO_3 is detected when molybdenum loading is equivalent or larger than a monolayer.

In general, the reducibility of molybdenum increases with the metallic loading, regardless the support used [36]. Nag [40] considers that at very low surface coverage, most of Mo remains in tetrahedral form. Its low reducibility allows that only a small fraction of total Mo generates species like the one shown in Scheme 3. To represent the MoO_x species we have used the model proposed by Nag [40].

It has been observed that the addition of Mo decreases the hydrogen adsorption capacity of Pd [41,18]. Oxidation at high temperatures favors MoO_3 formation. During reduction at high temperature, MoO_3 reduces to mobile suboxides (MoO_x), which are located on the palladium surface. Because of this, the MoO_x species was placed on Pd(1 1 1).

Following the data found in the literature [42], the Mo–O distance is fixed in 1.95 Å and the Mo=O bond length is 1.67 Å. This model is identified as MoO_x-Pd(1 1 1).

4.3. γ-Al_2O_3 surface

To represent the support, a γ-Al_2O_3 cluster was constructed. Hydrogen atoms complete the coordination of aluminum. It was considered that an alumina cluster of two layers is appropriate to model the support [43,47].

γ-Al_2O_3 model was built based on the tetragonally distorted defect spinel structure [44,45], with aluminum cations located in an approximately cubic close packed oxygen array. The exposed plane studied was (1 0 0). This plane, together with C and D faces of plane (1 1 0), is the preferred one [45,46]. Other planes as (1 1 1) could exist, but they are less abundant.

The model contains 111 atoms: 53 O, 12 Al and 46 H located as shown in Scheme 4 [47].

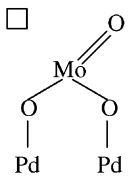

Scheme 3. MoO_x species on Pd surface.

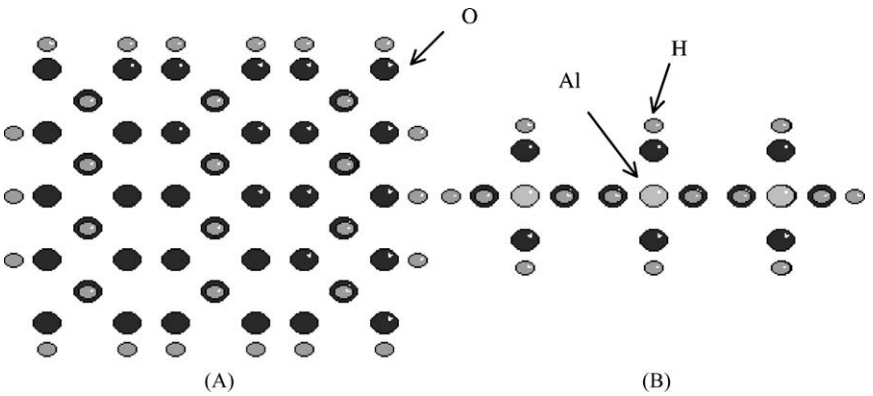

Scheme 4. γ-Al_2O_3(1 0 0) model: (a) top, and (b) lateral views.

4.4. MoO_x-γAl_2O_3 surface

In order to represent Mo/γ-Al_2O_3 catalyst partially reduced, a MoO_x structure (Scheme 3) was placed on (1 1 1) plane of γ-Al_2O_3. Keeping in mind the lattice parameter corresponding to γ-alumina and angles and bond lengths of MoO_x species, two hydrogen atoms were removed of OH surface groups to locate molybdenum species.

A cluster of 111 atoms was modeled: 54 O, 12 Al, 1 Mo and 44 H. This model was identified as MoO_x-γAl_2O_3 and it is shown in Scheme 5.

4.5. Adsorption of oxygen and nitrogen on Pd(1 1 1)

The adsorption and dissociation of nitrogen and oxygen molecules was studied due to their relevance in the NO decomposition reaction. N_2 and O_2 adsorption can be represented as:

$$O_2 \rightarrow O_2^{\bullet}$$

$$N_2 \rightarrow N_2^{\bullet}$$

where '•' represents the adsorption site on Pd(1 1 1).

Adsorption energy was calculated subtracting to the total energy of the adsorption system the energy corresponding to the free molecule and to the metallic cluster:

$$E_{ads} = E_{molecule/cluster} - E_{molecule} - E_{cluster}$$

Molecule–surface distance was optimized. In this work, the bond lengths in the adsorbed molecules remain fixed in all the calculations and they are detailed in Table 3 [48].

The molecule can adsorb either:

- perpendicular, molecular axis is normal to the surface; or

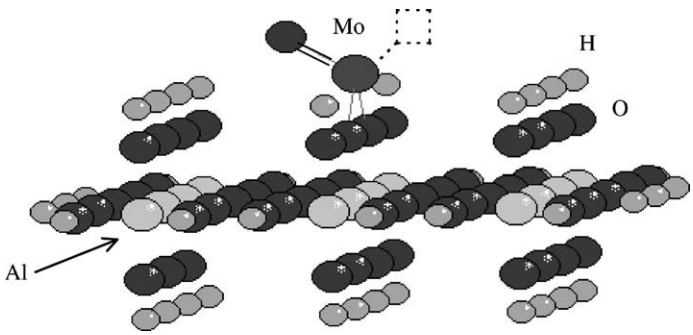

Scheme 5. MoO_x-γAl_2O_3(1 0 0) model.

Table 3
Bond lengths for studied molecules[a]

Molecule	Bond length (Å)
O_2	1.207
N_2	1.097
NO	1.150

[a] [48].

- parallel, molecular axis is parallel to the metallic surface.

The (1 1 1) face is the most compact in a fcc solid. Based on its coordination number, there are three possible sites for adsorption: 'on-top', 'bridge' and 'hollow'. In the last case, two possibilities should be considered: the molecule is located on a metallic atom of the second layer (hcp site) or it is on an atom belonging to third layer (site fcc). Scheme 1 shows adsorption sites location.

Scheme 6 presents three possible places of adsorption for the molecule when its orientation is vertical with regard to the palladium plane: (a) on-top, (b) bridging and (c) hollow sites.

Scheme 7 shows different configuration of adsorption for a horizontal molecule. Parts (a–c) as shown in Scheme 7 correspond to on-top site, when the molecule is approaching the adsorbing site by its symmetry center or by one of its ends, (d) and (e) refer to adsorption on a bridging site and (f) on a hollow site.

4.6. Dissociation of oxygen and nitrogen on Pd(1 1 1)

N_2 and O_2 dissociation can be represented as:

$$O_2^{\bullet} \rightarrow 2O^{\bullet}$$

$$N_2^{\bullet} \rightarrow 2N^{\bullet}$$

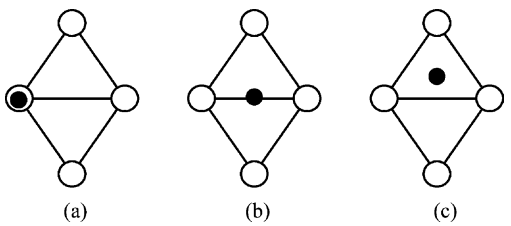

Scheme 6. Model of N_2, O_2 and NO adsorption on Pd(1 1 1). Molecular axis is normal to the surface.

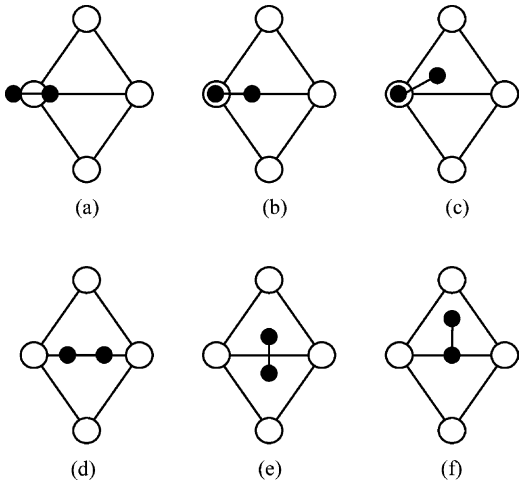

Scheme 7. Model of O_2 and N_2 over Pd(1 1 1). Molecular axis is parallel to the metallic surface.

The dissociation energy was calculated as follows:

$$E_{\text{dissociation}} = E_{\text{2N/cluster}} - E_{\text{N}_2\text{/cluster}}$$

where $E_{\text{N}_2\text{/cluster}}$ corresponds to the optimum value found during adsorption studies ($E_{\text{molecule/cluster}}$ in the previous paragraph).

4.7. NO adsorption on Pd(1 1 1)

As it was already said, at the adsorption step, two orientations of the incoming molecule are considered: perpendicular or parallel. There are three possible sites for the NO adsorption: on-top, bridge and hollow. Three possible adsorption sites for a vertically approaching molecule are presented in Scheme 6. Consistent with previous calculation results of adsorption energy [49,50], in the present work, the NO molecule approaches via the nitrogen atom onto the Pd(1 1 1) surface.

Scheme 8 presents different geometries for NO adsorption when the molecule is placed horizontally to the surface. Gray and black circles represent oxygen atoms and nitrogen atoms, respectively. In Scheme 8(a–c), NO is adsorbed on an on-top site. The adsorption site is contacted by the molecule symmetry center, the oxygen or the nitrogen atom, respectively. In Scheme 8(d) and (e), NO comes closer to a bridging site and, in Scheme 8(f) and (g) to a hollow site,

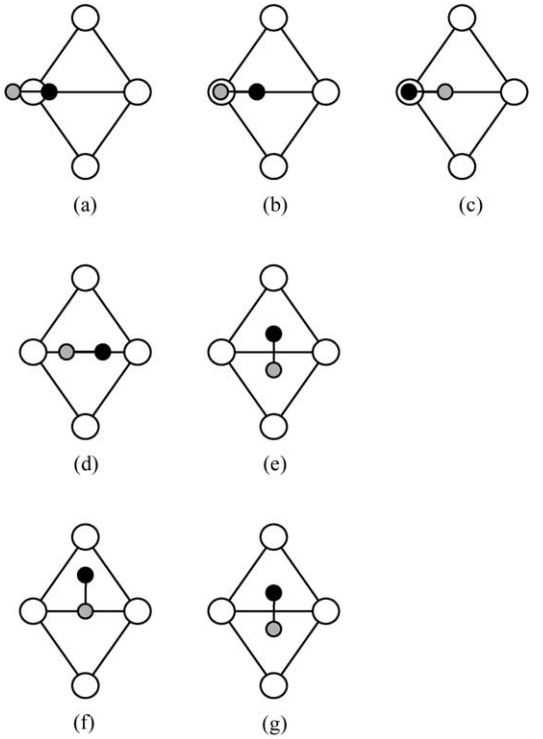

Scheme 8. Model of NO adsorption on Pd(1 1 1). Molecular axis is parallel to the metallic surface. Open and filled circles represent O and N atoms, respectively.

approaching by its symmetry center or by the nitrogen atom. The molecule–surface distance was optimized and the N–O distance (in the NO molecule) was kept constant at 1.15 Å (Table 3).

4.8. NO dissociation on Pd(1 1 1)

NO dissociation was studied on Pd(1 1 1). Dissociation energy was calculated as follows:

$$E_{\text{dissociation}} = E_{\text{N,O/cluster}} - E_{\text{NO/cluster}}$$

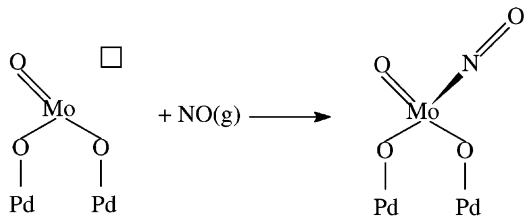

Scheme 9. Model of NO adsorption on MoO_x-Pd(1 1 1).

where $E_{\text{NO/cluster}}$ corresponds to the optimum value found during the NO adsorption study. Atom–surface distances were optimized: keeping constant the optimum N–surface distance (found for NO adsorption) and optimizing the O–surface distance. Then, maintaining the optimized O–surface distance, the minimum energy of the system is found, varying in the N–surface.

4.9. NO adsorption and dissociation on MoO_x-γAl_2O_3 and MoO_x-Pd(1 1 1) surfaces

The NO adsorption on MoO_x species was studied. The selected model to represent MoO_x was described before (Scheme 3). It has been considered that the NO molecule is adsorbed on a Mo atom in such a way that the MoO_x species preserves its tetrahedral coordination, as it is represented in Scheme 9. The N–O distance was maintained fixed at 1.15 Å.

Scheme 10 summarizes a possible NO dissociation on MoO_x. The calculations were carried out considering that the N atom is adsorbed on Mo with a N–Mo distance equal to the optimum value found during NO adsorption study, and varying the distance O–Mo.

4.10. N_2 and O_2 adsorption and dissociation on MoO_x-γAl_2O_3 and MoO_x-Pd(1 1 1) surfaces

The adsorption of N_2 and O_2 on MoO_x-Pd(1 1 1) and MoO_x-γAl_2O_3 has been studied. It was consid-

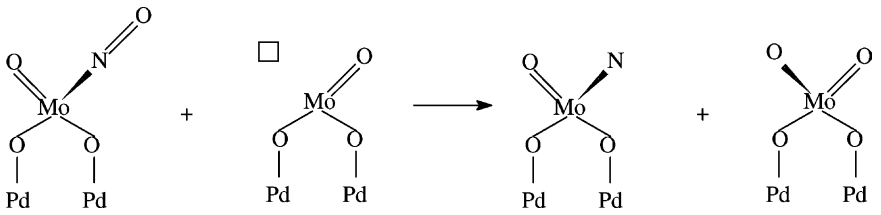

Scheme 10. Model of NO dissociation on MoO_x-Pd(1 1 1).

ered that these molecules were adsorbed on a Mo atom in a similar way to NO adsorption (retaining the tetrahedral coordination on molybdenum species and the bond length of the free molecules).

The dissociation over MoO_x was studied in a similar way as NO adsorption, using the optimum N–Mo and O–Mo distances found in adsorption calculations.

5. Results

5.1. Experimental

The results of the palladium exposed fraction calculated from H_2 chemisorption are listed in Table 1. In relation to the Pd/γ-Al_2O_3 catalyst, bimetallic samples show a decrease in the H_2 chemisorption capacity of palladium following molybdenum addition. High oxidation temperature favors the formation of MoO_3 that after exposure to pure H_2 at 300 °C, is reduced to suboxides that are claimed to migrate onto palladium surface impeding its contact with H_2 [41]. Similar results were reported for Ru-Mo samples [51,52] and Rh-Mo catalysts [53–55].

The TPR profiles of the catalysts are shown in Fig. 1. Those corresponding to Pd/γ-Al_2O_3 and to the bimetallic samples show a peak centered at ∼25 °C. This signal is assigned to the reduction of palladium oxide. The Pd/γ-Al_2O_3 catalyst presented a slightly lower temperature for the PdO reduction than the samples that were modified with molybdenum. The negative peak around 60 °C is attributed to palladium hydride decomposition. The small peak correlates well with the average particle size showed by the samples, since the hydride formation is a bulk phenomenon.

On the other hand, the TPR profile of Mo/γ-Al_2O_3 evidences a very low hydrogen consumption just before 500 °C. It is important to note that no change in sample color was observed (Mo sample is white after calcination and this color remains after the TPR experiment).

There are no important differences between Pd-Mo/γ-Al_2O_3 and Mo-Pd/γ-Al_2O_3 catalysts. The TPR profiles of bimetallic samples show a hydrogen consumption in the 80–200 °C temperature range. This broad peak would be related to highly dispersed palladium oxide, which is reduced at temperatures higher than

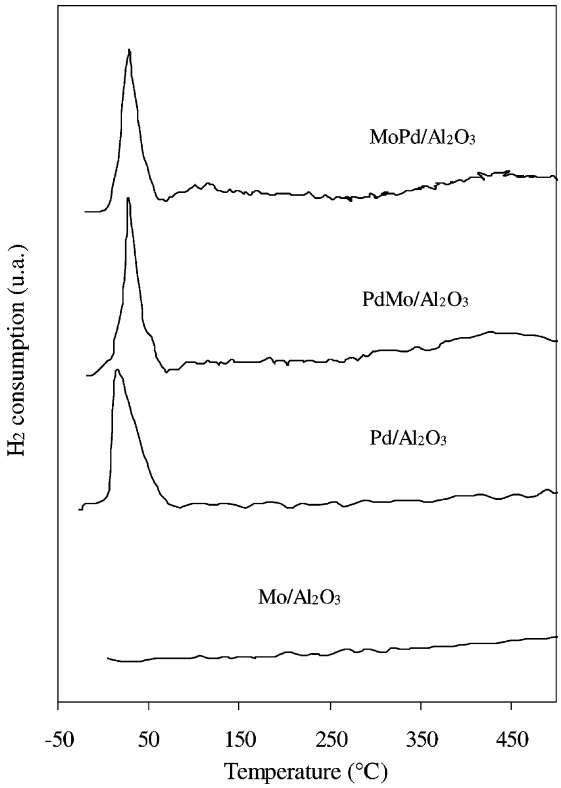

Fig. 1. TPR profiles. Oxidation temperature, 300 °C.

100 °C [56] or to Pd-Mo species, more strongly linked to the support than the PdO species, which would explain the reduction at higher temperature. Another possible explanation would be the bronze formation, due to the hydrogen spillover from the noble metal towards MoO_3 [57]. This H_2 consumption is not present in Pd/γ-Al_2O_3 sample and it demonstrates the interaction between palladium and molybdenum. Furthermore, the hydrogen consumption at high temperature corresponds to the partial reduction of molybdenum.

Fig. 2 presents NO conversion as a function of the reaction time, at 400 °C after a reduction treatment at 300 °C. Since the same palladium mass was used in the reaction, relative performances can be discussed. The Pd containing samples have presented a similar qualitative behavior: the initial NO decomposition was total and then it diminished gradually. The only observed products were N_2 and N_2O. It would indicate that the decrease of the activity in the time was originated by the oxygen retention on the catalytic surface.

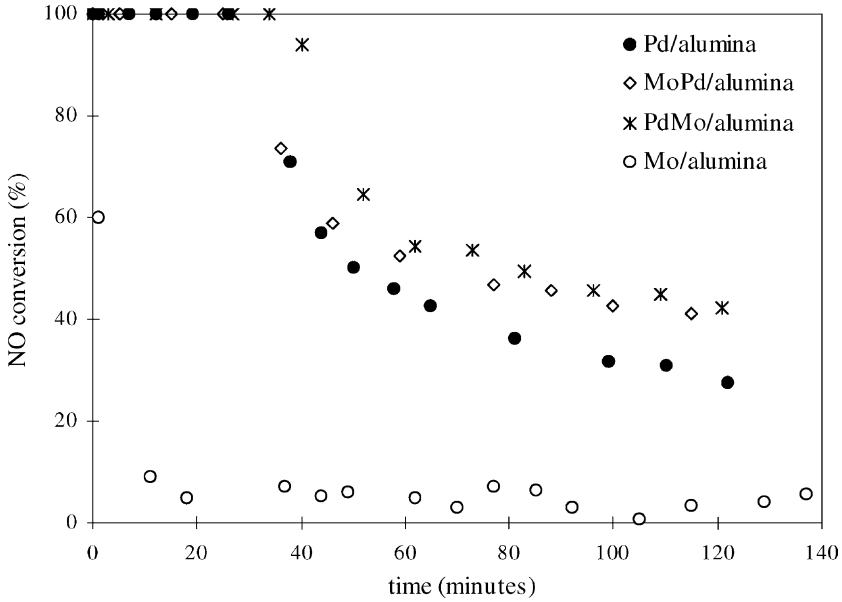

Fig. 2. NO conversion as a function of reaction time at 400 °C. SV = 4×10^4 mol of feed (h mol of Pd)$^{-1}$.

In all the cases, the nitrogen balance allowed to discard the possible formation of NO_2.

The Mo/γ-Al_2O_3 catalyst was not active for the NO decomposition. The activity fluctuated among 2–5% during the reaction time. A catalyst mass was used in such a way that the total content of Mo was similar to that used in the catalytic test of the Pd-Mo/γ-Al_2O_3 sample. According to the TPR results (Fig. 1), molybdenum is present as MoO_3 over the support after reduction at 300 °C.

The bimetallic samples have a better catalytic performance than the monometallic palladium sample. It is observed that Pd-Mo/γ-Al_2O_3 have exhibited a longer time working at very high conversions, and although they deactivate, the steady-state conversions after a reaction time of 120 min are higher. In these catalysts, the Mo reducibility increases (TPR profiles as shown in Fig. 1); therefore, there would be a higher proportion of MoO_x species in the Pd-Mo systems than in Mo/γ-Al_2O_3 catalyst. Oxygen vacancies or co-ordinative unsaturated sites (CUS) are postulated in [58–60] as the possible active site for NO decomposition on metallic oxides. Anderson et al. [61] studied Rh-MoO_3/γ-Al_2O_3 catalyst and found that although a small proportion of Mo could be reduced to MoO following high temperature reduction, cycles of high temperature reduction and oxidation produced Rh/Mo oxide phases in which a proportion of Mo could be reduced to MoO at 473 K. The presence of reduced Mo would appear to play an important role in the improved performance of Rh-MoO_3/γ-Al_2O_3 catalysts in NO_x decomposition reaction.

If the activities of Pd/γ-Al_2O_3, Mo/γ-Al_2O_3 and Pd-Mo/γ-Al_2O_3 systems are compared, it is found that those corresponding to the bimetallic one are not just the sum of the activities of the corresponding monometallics. Then, it should be considered that in the bimetallic catalysts the interaction between the metals is important and could affect the properties in the Pd–MoO_x interface. There are many examples about strong metal–support interaction (SMSI) effect on supported catalysts. Hussain [62] investigated the SMSI effect on supported Ru:Mn bimetallic catalyst supported on TiO_2. Their studies reveled that the CO chemisorption suppresses on the samples reduced at 723 K. The SSIMS technique indicates the presence of TiO_x species forming two new surface sites TiO_x-Ru and TiO-Mn. On TEM study, these new species were found to be located at the immediate vicinity of metal particles. Modifications were

observed on activity and product selectivity when theses species were present. According to the author, these new surface sites modify the surface geometry electronically. The results showed by Pande and Bell [63] demonstrated that NO chemisorption is suppressed with increasing catalyst reduction temperature for Rh/TiO_2 and TiO_2-promoted Rh/SiO_2. While this trend is similar to that observed for H_2 and CO chemisorption, the amount of NO adsorbed is significantly larger than the amount of H_2 and CO adsorbed. The suppression of NO, CO and H_2 chemisorption with increasing reduction temperature is believed to result from physical blockage of rhodium surface sites by TiO_x moieties transferred from the support. The higher adsorption capacity for NO relative to CO and H_2 is ascribed to NO adsorption on partially reduced sites present on portions of titania closely adjacent to Rh crystallites. These adsorption sites are formed by spillover of atomic hydrogen from Rh crystallites onto the support and consequent reduction of a portion of the support surface. A similar effect was found on Pd/CeO_2. According to the author, these new surface sites electronically modify the surface geometry. The same effect was found on Pd/CeO_2 [64], Pd/TiO_2 [65] and $Pd\text{-}Cu/NiO_2$ [66]. We consider a similar interaction between Mo and Pd, and as it will be shown, our theoretical results confirm this hypothesis.

5.2. N_2 and O_2 adsorption on Pd(1 1 1)

Tables 4 and 5 show the relative adsorption energy and optimum distances for N_2 and O_2 molecules adsorbed on Pd(1 1 1) surface. For each adsorption-site examined, it is only reported the geometry more energetically favored, which is indicated between parenthesis.

Table 4
Calculated relative energies (eV) and N–Pd distances (Å) for N_2 adsorbed on Pd(1 1 1)

Site	N_2 vertical		N_2 horizontal	
	E (eV)	d (Å)	E (eV)	d (Å)
On-top	−7.56	1.3	−2.61 (a)[a]	1.5
Bridging	−5.21	1.0	−10.13 (d)	1.0
Hollow fcc	−4.37	1.0	−7.89	0.8

[a] Diverse geometries were analyzed and the minimum energy value is reported. The letter between parenthesis refers to the corresponding figure of Scheme 7.

Table 5
Calculated relative energies (eV) and O-Pd distances (Å) for O_2 adsorbed on Pd(1 1 1)

Site	O_2 vertical		O_2 horizontal	
	E (eV)	d (Å)	E (eV)	d (Å)
On-top	−13.64	1.5	−13.29 (a)[a]	1.6
Bridging	−12.94	2.5	−18.95 (d)	1.1
Hollow fcc	−12.95	2.6	−16.89	1.0

[a] Diverse geometries were analyzed and the minimum energy value is reported. The letter between parenthesis refers to the corresponding figures of Scheme 7.

It was observed that adsorption values for hollow fcc and hollow hcp sites were equals. For this reason, we have only studied hollow fcc site as tri-coordinated place of adsorption.

Table 4 presents results for N_2 adsorption. The horizontal orientation is energetically favored on bridging site (figure (d) in Scheme 7).

Table 5 presents the relative energy and O–Pd distance for O_2 adsorption on Pd(1 1 1). N_2 and O_2 molecules are preferentially adsorbed on bridging site with horizontal orientation.

It was found that oxygen adsorption energy is higher than the one for nitrogen. This information agrees with experimental observations, since during NO decomposition, the catalyst surface is poisoned by oxygen retention.

5.3. N_2 and O_2 dissociation on Pd(1 1 1)

Table 6 presents the results obtained for dissociation. When the nitrogen molecule is dissociated, the atoms are located on bridging sites with a minimum

Table 6
Calculated relative energies (eV) and distances (Å) for N_2 and O_2 dissociation on Pd(1 1 1). In all cases, distances are reported to xy plane. Values of O implies that the atom is at the same height than Pd

Molecule	On-top[a]		Bridging[a]		Hollow[a]	
	E (eV)	d (Å)	E (eV)	d (Å)	E (eV)	d (Å)
O_2	−12.00	3.4	−12.00	3.2	−8.74	3.0
N_2	−12.55	1.3	−12.83	0.0[b]	0.06	0.1[c]

[a] Site.
[b] Pd–N=0.8 Å.
[c] $Pd\text{–}N_1$=1.35 Å and $Pd\text{–}N_2$=1.29 Å.

energy value, although it should be noticed that on-top sites present similar energy.

When the oxygen dissociation was studied, a well-defined minimum of energy was not found. The oxygen atoms are located preferably on-top and bridging sites.

Garda [67] observed that it was not possible to find a well defined minimum value for the total energy when she optimized N–O distance, in the NO molecule. She also found that the oxygen atom acquired an excess of negative charge that would increase the electron–electron repulsion. This can be related to parameters. However, because of the usage of the method, used as qualitative tool, this drawback does not affect the general trend.

Looking at the Pd–O distances for adsorption, the energy found for Pd on-top at a distance of 1.6 Å is closer to reported distances in PdO and PdO_2. Pd–O is 1.75 Å and 1.85 Å in PdO_2 [68]. In the case of 1.85 Å, it can be considered to be a double bond [69]. It seems that these oxygen atoms from NO decomposition are incorporated in the bulk and, thus cause oxidation of the highly dispersed Pt and Rh particles [70]. Xu and Goodman [10] studied NO decomposition over Pd catalysts and found that there was no detectable O_2 evolution below 1000 K for all sizes of Pd particles. However, O_2 desorption was observed in a peak at approximately 1250 K, concurrent with the desorption of Pd. Therefore, oxygen from NO decomposition was apparently dissolved into the bulk of the Pd particles. The long distance found at the dissociation step for O is related to the lack of relativistic effects in EHMO. It has been reported that it is very difficult to treat second-row metal oxides [69]. The partly covalent–ionic character of Pd–O can be a part of the problem, with an overestimation of electronic repulsion Pd–O by EHMO, because of the high number of d-electrons in Pd [68,69]. Even sophisticated methods are not powerful enough to represent the ground and excited states of oxides of high-occupied d-orbital atoms like Pd. Because of the structure of Mo, this problem does not arise (not filled d-orbitals).

5.4. NO adsorption on Pd(1 1 1)

NO adsorption was favored on on-top sites, with vertical orientation. The results are reported in Table 7.

Table 7
Calculated relative energies (eV) and N–Pd distances (Å) for NO adsorbed on Pd(1 1 1)

Site	NO vertical		NO horizontal	
	E (eV)	*d* (Å)	*E* (eV)	*d* (Å)
On-top	−13.61	1.3	−9.25 (c)[a]	1.6
Bridging	−11.62	0.8	−11.93 (d)	1.1
Hollow fcc	−10.53	0.8	−10.89 (f)	0.9
Hollow hcp	−10.42	0.8	−10.87 (f)	0.9

[a] Diverse geometries were analyzed and the minimum energy value is reported. The letter between parenthesis refers to the corresponding figures of Scheme 8.

When the molecule is adsorbed with vertical orientation, it can be observed that the relative energies are a decreasing function of the coordination number.

Wickham et al. [71], using EELS, showed that for saturation coverage of NO on Pd(1 1 1) at −173 °C, NO co-exists adsorbed on on-top and two-fold bridge sites.

Hoost et al. [72] investigated the NO adsorption on 2 wt.% Pd/γ-Al_2O_3 using IR at 25 °C. They found that NO adsorbs in linear form over the reduced catalyst, while on oxidized sample it was detected that NO connected two- and three-folds.

5.5. NO dissociation on Pd(1 1 1)

In Table 8, the obtained results are shown. For the sake of simplicity, we have only considered two possible adsorption sites: on-top and bridged. These sites present the smallest energy of NO adsorption (Table 7). The dissociation energy is slightly higher when N is placed in on-top site. Again, a well defined minimum of energy for the oxygen atom was not found.

Table 8
Calculated relative energies (eV) and distances (Å) for NO dissociation on Pd(1 1 1)

N *d* (Å)		O *d* (Å)		*E* (eV)
On-top	Bridging	On-top	Bridging	
1.3		3.4		−12.36
1.3			3.6	−12.35
	0.0	3.4		−12.09
	0.0		3.6	−12.09

Table 9
Calculated relative energies (eV) and distances (Å) for NO adsorbed on MoO_x-γAl_2O_3 and MoO_x-Pd(1 1 1) models

	E (eV)	d (A)
N → Mo		
MoO_x-γAl_2O_3	−8.27	1.4
MoO_x-Pd(1 1 1)	−17.47	1.3
O → Mo		
MoO_x-γAl_2O_3	−6.31	1.4
MoO_x-Pd(1 1 1)	−10.53	1.4

5.6. NO adsorption and dissociation on MoO_x-γAl_2O_3 and MoO_x-Pd(1 1 1) surfaces

Table 9 shows the relative energy and distance when the NO molecule is adsorbed on a Mo atom (MoO_x species maintains the tetrahedral coordination and the N–O distance is 1.15 Å). The calculations have indicated that the molecule would approach to Mo by its N atom. The relative energy corresponding to MoO_x-Pd(1 1 1) model is higher than MoO_x-γAl_2O_3 (9.2 eV).

Scheme 10 represents the NO dissociation on MoO_x species. The results of EHMO calculations in this topic are given in Table 10. Our results seem to indicate that it is energetically probable. NO dissociation on Mo is easier for MoO_x-Pd(1 1 1) model than if molybdenum is over alumina (−9.48 eV versus −4.44 eV). The close contact between Mo and Pd favors the adsorption and dissociation of NO.

5.7. N_2 and O_2 adsorption and dissociation on MoO_x-γAl_2O_3 and MoO_x-Pd(1 1 1) surfaces

The results are presented in Table 11. Adsorption energies of N_2 on MoO_x are similar in the two models studied (approximately −11 eV). When the molecule is oxygen, there is an important difference in the values: −4.79 eV for MoO_x-γAl_2O_3 and −17.34 eV for MoO_x-Pd(1 1 1).

Table 10
Calculated relative energies (eV) and distances (Å) for NO dissociation on adsorbed on MoO_x-γAl_2O_3 and MoO_x-Pd(1 1 1) models.

Model	E (eV)	N–Mo d (Å)	O–Mo d (Å)
MoO_x-γAl_2O_3	−4.44	1.4	1.3
MoO_x-Pd(1 1 1)	−9.48	1.3	1.1

Table 11
Calculated relative energies (eV) and distances (Å) for N_2 and O_2 adsorbed on MoO_x-γAl_2O_3 and MoO_x-Pd(1 1 1) models

	E (eV)	d (Å)
N_2		
MoO_x-γAl_2O_3	−11.47	1.5
MoO_x-Pd(1 1 1)	−11.03	1.3
O_2		
MoO_x-γAl_2O_3	−4.79	1.4
MoO_x-Pd(1 1 1)	−17.34	1.2

Table 12
Calculated relative energies (eV) and distances (Å) for N_2 and O_2 dissociation on MoO_x-γAl_2O_3 and MoO_x-Pd(1 1 1) models

	E (eV)	d (Å)
N		
MoO_x-γAl_2O_3	−5.60	1.4
MoO_x-Pd(1 1 1)	−13.27	1.1
O		
MoO_x-γAl_2O_3	−3.11	1.4
MoO_x-Pd(1 1 1)	−12.00	1.2

Dissociation energies are collected in Table 12. The values differ notably with the models for both the studied molecules. The Pd–Mo interaction causes an increase in the dissociation energy and a decrease in atom–surface distances.

6. Discussion and conclusions

The difference '$E_{\text{dissociation}} - E_{\text{adsorption}}$' is the relative formation energy of the molecule from its adsorbed atoms on the catalyst. Considering the Pd(1 1 1) model and the horizontal mode of adsorption on bridge sites, the value is −2.70 eV for nitrogen and +6.95 eV for oxygen (as shown in Tables 4–6). According to experimental evidence, these results indicate that adsorbed N atoms form N_2, while oxygen atoms poison the Pd catalyst surface.

The O_2 adsorption on Pd is energetically favored with regard to that of NO (−18.95 versus −13.60 eV). These results explain the quick poisoning of the catalyst during the reaction of NO decomposition.

When the NO molecule has been analyzed, it was found that adsorption and dissociation energies

for Pd(1 1 1) model are higher than the ones for MoO_x-γAl_2O_3. This result agrees with the experimental results obtained for Pd/γ-Al_2O_3 and Mo/γ-Al_2O_3 catalysts (Fig. 2). Adsorption is from N-side whatever the surface. Dissociation energies are almost 2.8 times higher for Pd(1 1 1), as shown in Tables 8 and 10.

On the other hand, our results of EHMO calculations have showed that the catalytic properties of Mo supported on γ-alumina differ notably of Mo in contact with Pd. This Pd–Mo interaction was evident in the TPR experiments as well as in hydrogen chemisorption. This can be related to the changes due to Pd–Mo close contact.

The NO adsorption energy on MoO_x-Pd(1 1 1) is higher than the one for Pd(1 1 1) or MoO_x-γAl_2O_3. Also adsorption and dissociation of N_2 and O_2 are modified notoriously when an interaction exists between the two metals. For nitrogen molecule, the difference '$E_{\text{dissociation}} - E_{\text{adsorption}}$' is 5.87 eV for MoO_x-γAl_2O_3 model and −2.54 eV for MoO_x-Pd(1 1 1). It indicates that N atoms are more easily desorbed forming N_2 in the bimetallic sample. These results are important, and they would indicate the existence of an interface Pd-Mo with catalytic properties different to the metals taken separately.

In terms of stability and NO conversion (as shown in Fig. 2), the order is:

Pd-Mo > Mo-Pd > Pd > Mo

The strength of the NO-surface bond at adsorption decreases in the order:

MoO_x-Pd(1 1 1) > Pd(1 1 1) > MoO_x-γAl_2O_3

The dissociation energy follows the trend:

Pd(1 1 1) > MoO_x-Pd(1 1 1) > MoO_x-γ-Al_2O_3

Actually, Pd-Mo catalysts can be seen as MoO_x supported on Pd(1 1 1) and, therefore, some kind of SMSI takes place. It seems that the sticking coefficients of NO for MoO_x-Pd(1 1 1) is higher than for Pd(1 1 1) and, therefore, the activity would be higher.

Differences between the first two surfaces can be related to exposed Pd (as shown in Table 1). It seems that Pd-Mo has the best combination of conditions to optimize performance. It is clear from Scheme 2 that MoO_x occupies bridging sites on Pd(1 1 1). The relative amount of on-top Pd increases on Pd(1 1 1) exposed, being present MoO_x. These facts could be related to preferentially exposed on-top Pd in Pd-Mo, where N_2 formation would be favored in −9.94 eV, whereas, O_2 formation has an energy of +1.29 eV. For NO, adsorption of NO horizontal (a needed step for dissociation) has an energy of −9.25 eV instead of −11.93 eV for pure Pd(1 1 1). In this case, NO adsorption is not so favored as in case of Pd(1 1 1). The resulting increase in activity could be a compromise between both effects from both the metals Pd and Mo: lower adsorption energy for NO on Pd(1 1 1) in bimetallic sample and an even much lower adsorption energy for the product N_2 once formed. The effect is clear on Mo: NO adsorption is strongly favored versus pure Pd, but not dissociation. For N_2 as product, the result is the same as in the case of Pd in Pd-Mo. The fact that the required energies for O_2 formation decreases in the order:

$$\text{Pd(1 1 1)}_{\text{bridging}} > \text{Pd-MoO}_x > \text{Pd(1 1 1)}_{\text{on-top}}$$

can be related to higher stability (and then lower poisoning effect of oxygen) when Pd-Mo is analyzed.

Kao et al. [73] considered that the top-site NO on Rh(1 1 1) either desorbs or shifts to bridge-site NO instead of dissociating; however, the bridge-site NO is the major contributor to the dissociation of NO to atomic oxygen and nitrogen in the temperature range of 350–480 K. Similar findings were reported on Ru(0 0 1) [74]. The adsorption of NO on Pd/MgO(1 0 0) model catalyst has been studied by Piccolo and Henry [75], in the temperature range of 430–700 K, for various cluster sizes (d = 2.8–45 nm), using pulsed molecular beam. The ability of a Pd surface to dissociate NO is highly structure-sensitive. On a perfect Pd(1 1 1) surface, NO adsorbs molecularly [76]. Molecular adsorption and dissociation strongly compete on Pd(1 0 0) [77] and Pd(1 1 0) [78] surfaces. The degree of dissociation is much higher on stepped Pd(1 1 1) [79]. These supported model catalysts are more suited for understanding of size and support effects in catalysis. For all the studied samples, whatever the particle size (15.6, 6.6 and 3.1 nm) the measured rates of nitrous oxide (N_2O) formation is so low that it can be considered as negligible, contrary to the observation made by Xu and Goodman [10] and Goodman and co-workers [81] on SiO_2 and Al_2O_3 supported Pd catalysts [80]. This discrepancy

probably originates from the differences in cluster shapes, which are strongly substrate-dependent.

The adsorption behavior of NO on Pd(1 1 1) surface appeares to be similar to that on Rh(1 1 1). HREELS studies indicated that the adsorption site of NO on Pd(1 1 1) depends on surface temperature and coverage [73]. Bridge-site NO populates first at both 130 K and room temperature; but top-site NO exists only below 250 K at high surface coverage on Pd(1 1 1). At room temperature, all the top-site NO desorbs first, followed by bridge-site desorption at 400 K. Because of steric reasons, vertical NO would be favored at high NO coverages. Comparing the energies, horizontal NO is energetically favored for the sites, except for on-top. Being available, NO prefers vertical adsorption on-top but if these are not, horizontal NO is favored. The change from vertical to horizontal on-top is needed for dissociation. In this sense, horizontal NO can be seen as a transition state. Taking this fact into consideration, it is evident that on-top Pd(1 1 1) dissociation would be activated with high activation energy, whereas, on the other sites (bridging and hollow), the activation energies would be lower. The experimental facts are in line with this.

This analysis can explain our experimental results. Activity in Pd-Mo is not so high because, although the on-top Pd(1 1 1) sites relative concentration increases and vertical NO adsorption is favored, the activation for NO dissociation would be higher.

The experimental differences observed in the catalytic tests for Pd/Al_2O_3 and $Pd\text{-}Mo/\gamma\text{-}Al_2O_3$ samples would be consequences of the presence of new MoO_x–Pd interface with different properties to those observed in the metals separately and the existence of higher number of CUS on molybdenum surface (according to TPR results). The higher activities for Pd-Mo seem to be kinetic in nature: higher stability of active phase and a decrease of the poisoning effect of O on Pd. The O can be oxidizing Mo instead.

In view of the obtained results, we could ask what would happen if Pd-Mo catalyst were exposed to a gas-stream containing NO and some reducing agent. The SCR of NO_x by hydrocarbons is an attractive technique for NO_x control. One of the hydrocarbons of interest is methane, the chief component of natural gas. Burch and Scire [7] reported that the NO and CH_4 reaction on Pd catalysts takes place via NO adsorption and dissociation on metallic Pd sites forming N_2, whereas, the O generated is retained in the catalyst surface and is removed by reaction with CH_4, regenerating the active sites. In agreement with this, it would appear that the addition of Mo generates new sites for the adsorption and dissociation of NO, the first step of the mechanism. Now, the question is if the oxygen taken up by the MoO_x species will be removed by methane, or if these new sites will be poisoned during the course of the reaction.

The SCR of NO to N_2 by hydrocarbons in the presence of excess oxygen is an important commercial process for removing of pollutants from exhaust fumes. Pd catalyst is very active for the total oxidation of methane [82,83,22]. This is one of the major impediments for the use of methane as a reductant for the catalytic NO conversion (particularly in lean mixtures): its low selectivity towards the reaction with NO in competition with O_2 [84,85]. However, in recent years, several authors [8,86,87] have shown that when Pd is supported on acidic materials it can be active for the selective reduction of NO with CH_4. Chin and Resasco [88] and Resasco and co-workers [89] demonstrated that the morphology of the Pd species, under SCR reaction conditions, strongly depends on both, the metal loading and the acidity of the support. On low Pd-loading catalysts over acidic supports the metallic Pd particles, initially present on the catalyst, are rapidly transformed into Pd^{2+} ions by the reaction mixture. By contrast, on non-acidic materials, the Pd particles are transformed into PdO clusters, which have high activity for methane combustion. In view of these preceding works, Pd-Mo catalysts would be a possible alternative for the SCR of NO by CH_4, considering that the molybdenum addition increases the acidity of the Pd/alumina catalyst.

Considering the results presented in this paper, the goal of future works will be to study $NO + CH_4$ and $NO + CH_4 + O_2$ reaction over $Pd\text{-}Mo/\gamma\text{-}Al_2O_3$ catalysts, using experimental and theoretical techniques.

Acknowledgements

We acknowledge Professor Alfredo Juan of Universidad Nacional del Sur, Departamento de Física, for providing the modified version of ICONC and for helpful advice. We thank the Universidad Nacional del Sur (UNS) and the Consejo Nacional de

Investigaciones Científicas y Técnicas (CONICET) for their financial support. We thank Professor Mara Volpe for language checking.

References

[1] J. Armor, Appl. Catal. B 1 (1992) 221.
[2] A. Walker, Catal. Today 26 (1995) 107.
[3] V. Parvulescu, P. Grange, B. Delmon, Catal. Today 46 (1998) 233.
[4] A. Fritz, V. Pitchon, Appl. Catal. B 13 (1997) 1.
[5] B. Cho, B. Shanks, J. Bailey, J. Catal. 115 (1989) 486.
[6] A. Pisanu, Thesis, U.N.S., 1997.
[7] R. Burch, S. Scire, Appl. Catal. B 3 (1994) 295.
[8] C. Loughran, D. Resasco, Appl. Catal. B 5 (1995) 351.
[9] R. McCabe, C. Wong, J. Catal. 121 (1990) 422.
[10] X. Xu, D. Goodman, Catal. Lett. 24 (1994) 31.
[11] M. Valden, J. Aaltonen, E. Kausisto, M. Perra, C. Barnes, Surf. Sci. 307–309 (1994) 193.
[12] A. El Hamadaoui, G. Bergeret, J. Massardier, M. Primet, A. Renouprez, J. Catal. 148 (1994) 47.
[13] T. Hoost, G. Graham, M. Shelef, O. Alexeev, B. Gates, Catal. Lett. 38 (1996) 57.
[14] H. Gandhi, H. Yao, H. Stepien, Catalysis Under Transient Conditions, in: A.T. Bell, Y.L. Hedegies (Eds.), ACS Symposium Series no. 178, Am. Chem. Soc., Washington DC, 1982, p. 143.
[15] I. Halaz, A. Bremmer, M. Shelef, Appl. Catal. B 2 (1993) 131.
[16] I. Halaz, A. Bremmer, M. Shelef, Catal. Lett. 16 (1992) 311.
[17] I. Halaz, A. Bremmer, M. Shelef, Catal. Lett. 18 (1993) 289.
[18] M. Schmal, M. Baldanza, M. Vannice, J. Catal. 185 (1999) 138.
[19] L. de Mello, M. Baldanza, F. Noronha, M. Schmal, Studies in Surface Science and Catalysis, vol. 130, in: A. Corma, F. Melo, S. Mendioroz, J. Fierro (Eds.), Elsevier, Amsterdam, 2000, p. 647.
[20] A. Pisanu, C. Gigola, Appl. Catal. B. 11 (1996) L37.
[21] J. Benson, H. Hwang, M. Boudart, J. Catal. 30 (1973) 146.
[22] G. Tonetto, M. Ferreira, D. Damiani, J. Mol. Catal. A 171 (2001) 123.
[23] R. Hoffmann, J. Chem. Phys. 39 (6) (1963) 1397.
[24] R. Sumerville, R. Hoffmann, J. Am. Chem. Soc. 98 (1976) 23.
[25] P. Hay, J. Thibeault, R. Hoffmann, J. Am. Chem. Soc. 97 (1975) 4884.
[26] I. Chamber, L. Forrs, G. Calzaferri, J. Phys. Chem. 93 (1989) 5366.
[27] A. Anderson, R. Hoffmann, J. Chem. Phys. 60 (1974) 4271.
[28] W. Lotz, J. Opt. Soc. Am. 60 (1970) 206.
[29] A. Vela, L. Gázquez, J. Phys. Chem. 92 (1985) 5366.
[30] M. Ferreira, N. Castellani, D. Damiani, A. Juan, J. Mol. Catal. Part A. Chem. 122 (1997) 25.
[31] M. Ferreira, D. Damiani, A. Juan, Comput. Mat. Sci. 9 (1998) 357.
[32] E. Garbowski, C. Feumi-Jantou, N. Mouaddib, M. Primet, Appl. Catal. A 109 (1994) 277.
[33] T. Ward, P. Alemany, R. Hoffmann, J. Phys. Chem. 97 (29) (1993) 7691.
[34] A. Rochefort, J. Andzelm, N. Russo, D. Salahub, J. Am. Chem. Soc. 112 (23) 1990.
[35] L. Wang, W. Hall, J. Catal. 66 (1980) 251.
[36] S. Rajagopal, H. Marini, J. Marzari, R. Miranda, J. Catal. 147 (1994) 417.
[37] J. Medema, C. van Stam, V. de Beer, A. Konings, D. Koningsberger, J. Catal. 53 (1978) 386.
[38] D. Zingg, L. Makovsky, R. Tischer, F. Brown, D. Hercules, J. Phys. Chem. 84 (1980) 2898.
[39] C. Williams, J. Ekerdt, J. Jehng, F. Hardcastle, I. Wachs, J. Phys. Chem. 95 (1991) 8791.
[40] N. Nag, J. Catal. 92 (1985) 432.
[41] L. Konopny, A. Juan, D. Damiani, Appl. Catal. B 15 (1998) 115.
[42] L. Kihlborg, A. Kemi, 21 (1963) 357; G. Mestl, Catal. Rev. Sci. Eng. 40(4) (1998) 451.
[43] C. Pisani, M. Causa, R. Dovesi, C. Roetti, Prog. Surf. Sci. 25 (1987) 119.
[44] S. Wilson, J. Mc Connel, J. Phys. Chem. 34 (1980) 315.
[45] H. Konizinger, X. Ratnasamy, Catal. Rev. 17 (1978) 31.
[46] T. Shay, L.-Y. Hsu, J. Basset, S. Shore, J. Mol. Catal. 86 (1994) 479.
[47] M. Ferreira, M. Volpe, J. Mol. Catal. A 149 (1999) 33.
[48] D. Lide (Ed.), Handbook of Chemistry and Physics, 76th Edition, 1995/1996.
[49] F. Garin, Appl. Catal. A 222 (2001) 183.
[50] N. Greenwood, A. Earnshaw, Chemistry of the Elements, 2nd Edition, Butterworths, London, 2001, pp. 443, 452.
[51] A. Juan, D. Damiani, J. Catal. 137 (1992) 77.
[52] A. Juan, D. Damiani, Catal. Today 15 (1992) 169.
[53] N. Takahashi, T. Mori, A. Miyamoto, T. Hattori, Y. Murakami, Appl. Catal. 38 (1988) 301.
[54] N. Bhore, K. Bischoff, W. Manogue, G. Mills, New Catalytic Materials in Fuels Processing, American Chemical Division, ACS Symposium Series, Washington DC, 1990.
[55] B. Kip, E. Hermans, J. van Wolput, N. Hermans, J. van Grondelle, R. Prins, Appl. Catal. 35 (1987) 109.
[56] H. Lieske, J. Volter, J. Phys. Chem. 89 (10) (1985) 1842.
[57] P. Sermon, G. Bond, J. Chem. Soc., Faraday Trans. 1 (72) (1976) 730.
[58] E. Winter, J. Catal. 22 (1971) 158.
[59] T. Yamashita, A. Vannice, J. Catal. 163 (1996) 158.
[60] J. Hightower, D. van Leirsburg, The Catalytic Chemistry of Nitrogen Oxides, in: R. Klimisch, J. Larson (Eds.), Plenum, New York, 1975, p. 63.
[61] J. Anderson, A. Guerrero-Ruiz, J. Fierro, Topic Catal. 1 (1,2) (1994) 123.
[62] S. Hussain, J. Trace Microprobe Technol. 14 (2) (1996) 367.
[63] N. Pande, A. Bell, J. Catal. 97 (1986) 137.
[64] S. Naito, S. Aide, T. Tsunematsu, T. Miyao, Chem. Lett. 9 (1998) 941.
[65] M. Bowker, P. Stone, R. Bennett, N. Perkins, Surf. Sci. 497 (2002) 155.

[66] M. Pereira, F. Noronha, M. Schmal, Catal. Today 16 (1993) 407.
[67] G. Garda, Thesis, UNS, 2000.
[68] A. Dedieu, Chem. Rev. 100 (2) (2000) 543.
[69] K. Huber, G. Herzberg, Molecular Spectra and Molecular Structure, Van Nostrand Reinhold, New York, 1979.
[70] P. Loof, B. Kasemo, S. Andersson, A. Frestad, J. Catal. 130 (1991) 181.
[71] D. Wickham, B. Banse, B. Koel, Surf. Sci. 243 (1991) 83.
[72] T. Hoost, K. Otto, A. Laframboise, J. Catal. 155 (1995) 303.
[73] C.-T. Kao, G.S. Blackman, M.A. Van Hove, G.A. Somorjai, C.-M. Chan, Surf. Sci. 224 (1989) 77.
[74] H. Conrad, R. Scala, W. Stenzel, R. Unwin, Surf. Sci. 145 (1984) 145.
[75] L. Piccolo, C.R. Henry, Surf. Sci. 452 (2000) 198.
[76] R. Ramsier, Q. Gao, H. Neergaard Waltenburg, K.-W. Lee, O. Nooij, L. Lefferts, J. Yates Jr., Surf. Sci. 320 (1994) 209.
[77] S. Sugai, H. Watanabe, T. Kioka, H. Miki, K. Kawasaki, Surf. Sci. 259 (1991) 109.
[78] R. Sharpe, M. Bowker, Surf. Sci. 360 (1996) 2.
[79] H. Schmick, H.-W. Wassmuth, Surf. Sci. 123 (1982) 471.
[80] M. Hirsimaki, S. Suhonen, J. Pere, M. Valden, M. Pessa, Surf. Sci. 402 (1998) 187.
[81] D. Rainer, S. Vesecky, M. Koranne, W. Oh, D. Goodman, J. Catal. 167 (1997) 234.
[82] M. Lyubovsky, L. Pfefferle, Appl. Catal. A 173 (1998) 107.
[83] R. Burch, F. Urbano, Appl. Catal. A 124 (1995) 121.
[84] M. Iwamoto, H. Yahiro, Catal. Today 22 (1994) 5.
[85] M. Iwamoto, H. Hamada, Catal. Today 10 (1991) 57.
[86] Y. Nishizaka, M. Misono, Chem. Lett. (1993) 1295.
[87] Y. Nishizaka, M. Misono, Chem. Lett. (1994) 2237.
[88] Y. Chin, D. Resasco, Catalysis, Roy. Soc. Chem., London 14 (1999).
[89] Y.-H. Chin, A. Pisanu, L. Serventi, W. Alvarez, D. Resasco, Catal. Today 54 (1999) 419.